Journal of
Materials Chemistry A

Accepted Manuscript

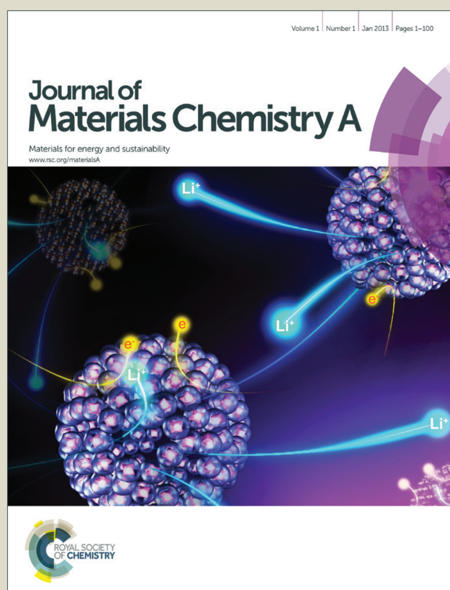

This is an *Accepted Manuscript*, which has been through the Royal Society of Chemistry peer review process and has been accepted for publication.

Accepted Manuscripts are published online shortly after acceptance, before technical editing, formatting and proof reading. Using this free service, authors can make their results available to the community, in citable form, before we publish the edited article. We will replace this *Accepted Manuscript* with the edited and formatted *Advance Article* as soon as it is available.

You can find more information about *Accepted Manuscripts* in the Information for Authors.

Please note that technical editing may introduce minor changes to the text and/or graphics, which may alter content. The journal's standard Terms & Conditions and the Ethical guidelines still apply. In no event shall the Royal Society of Chemistry be held responsible for any errors or omissions in this *Accepted Manuscript* or any consequences arising from the use of any information it contains.

ROYAL SOCIETY OF CHEMISTRY

www.rsc.org/materialsA

Journal of Materials Chemistry A Accepted Manuscript

High Efficiency PTB7-based Inverted Organic Photovoltaics on Nano-ridged and Planar Zinc Oxide Electron Transport Layers

By *Beau J. Richardson, Xuezhen Wang, Abdulrahman Almutairi* and *Qiuming Yu**

[*] Prof. Q.M. Yu., B.J. Richardson, X. Wang, A. Almutairi
Department of Chemical Engineering
University of Washington
Seattle, WA 98195, USA
Email: qyu@uw.edu
Phone: 206-543-4807

Inverted organic photovoltaics (OPVs) have gained considerable attention as they offer increased device stability and processing advantages. ZnO serves as an effective electron transport layer (ETL) in inverted OPVs while efficiently blocking holes. In this work, the sol gel precursor concentration, spin coating speed and baking conditions were used to simultaneously control the film thickness and morphology of ZnO ETLs in inverted devices using the active layer of poly thieno[3,4-b]thiophene/benzodithiophene (PTB7):[6,6]-phenyl C71-butyric acid methyl ester ($PC_{71}BM$) bulk heterojunction (BHJ). Nano-ridged and planar structures of ZnO films were obtained simply by dynamically and statically baking the precursor films, respectively. Consistently high FF's exceeding 70% and PCEs averaging 7.65-8.01% with a maximum PCE reaching 8.32% were achieved on both nano-ridged and planar ZnO films when the active layer was maintained at ~94 nm. The effects of ZnO film thickness and morphology, along with the active layer thickness, on the device performance were further investigated using both experimental and transfer matrix optical modeling methods. The results demonstrated that high efficiency PTB7-based inverted OPVs can be achieved on both nano-ridged and planar ZnO ETLs as long as the optimal active layer thickness is maintained.

1. Introduction

Organic photovoltaic cells (OPVs) with the inverted structure have been of peak interest in recent years due, in part, to better ambient stability and device processing advantages. In inverted devices, it is important to prepare a selective bottom cathode to effectively reverse the device polarity from a conventional to an inverted structure.[1, 2] This is typically achieved by forming an electron transport layer (ETL) on indium tin oxide (ITO). This ETL should have good optical transparency, low resistivity for electron conduction, and an appropriate conduction band (CB) level and bandgap (E_g) for high selectivity of electrons while also blocking holes. Various wide bandgap, n-type metal oxides, such as TiO_2, ZnO, Cs_2CO_3, and certain polyelectrolytes with a large dipole moment have been successfully deployed as interfacial ETLs in inverted devices.[1, 3-6] Additionally, varied forms of layer nanostructuring, surface treatment, and processing additives have been explored to improve charge collection efficiency, transport and selectivity.[7-10]

ZnO has drawn much attention as an ETL as it has high transparency in the visible region (E_g = ~3.3 eV)[1, 11-13], good electron mobility, proper energy level alignment with fullerene acceptors [13], environmental stability, low cost and is easily deposited via various solution processes [2]. This ease of processing and relative material abundance also makes ZnO a good candidate for large scale manufacturing. Good operational stability of inverted OPVs with ZnO ETLs has also been noted and attributed to the fact that ZnO blocks the UV light resulting in negligible UV-light-induced photodegradation of organic materials.[2]

Inverted devices can use ZnO films processed by various methods including atomic layer deposition (ALD) [14], sputtering [15], depositing pre-synthesized nanoparticles [5, 16] and sol gel techniques [3, 5, 10, 14]. Sol gel techniques can be advantageous because they are solution based,

Journal of Materials Chemistry A Accepted Manuscript

unlike ALD or sputtering, and do not involve the more complex synthesis steps required with nanoparticles. Additionally, metal oxide nanoparticles may form more porous and poorly interconnected particulate films at low processing temperatures.[3] Sol gel techniques are often used with widely ranging baking conditions to create dense and pin-hole free ZnO films with varying degrees of crystallinity.[1, 12, 17] For sol gel methods, the choice of precursor materials, concentration, spin coating speed, drying and baking steps all affect the optical, electrical, and structural properties of the films.[12] Interestingly, the morphology of sol-gel derived ZnO ETLs can be controlled to form a planar or a nano-ridged structure simply by static or dynamic (i.e. ramped-up) baking conditions, respectively.[3, 10]

Nano-ridged and planar ZnO structures were deployed in inverted devices using the poly(3-hexylthiophene) (P3HT):[6,6]-phenyl C_{61} butyric acid methyl ester ($PC_{61}BM$) bulk heterojunction (BHJ) active layer exhibiting a power conversion efficiency (PCE) as high as 4.0% for the dynamically baked devices versus 3.2% for the statically baked ones.[10] A high fill factor (FF) increase was observed while the open circuit voltage (V_{OC}) and short circuit current density (J_{SC}) stayed almost the same. This was attributed, in part, to lower current leakage and better charge selectivity due to a more densely packed ZnO film for the nano-ridged versus the planar morphologies stemming from the slower heating process. By comparing P3HT:ZnO bilayer devices, a large J_{SC} increase was observed with the nano-ridged structure indicating more interfacial area for charge separation also plays a role in the improvement. Both the dynamically and statically baked ZnO films were prepared using a precursor concentration of 0.75 M, spin speed of 2000 rpm, and a baking temperature of 275˚C. The dynamically baked films used a ramp rate of 50˚C/min to make ZnO nano-ridges.

Journal of Materials Chemistry A Accepted Manuscript

In another study, sol gel-derived ZnO films were dynamically and statically baked at a lower temperature (200˚C) and the spin coating time was varied to analyze both morphology and internal nanocrystal (NC) orientation.[3] A precursor concentration of 0.45 M and spin speed of 4000 rpm were used. Static baking was observed to create higher (002) plane NC orientation which is known to enhance lateral charge transport parallel to the device substrate. Dynamic baking created a more random crystal orientation that tended to support charge transport perpendicular to the substrate benefitting overall charge transport. Due to the experimental conditions, the formation of nano-ridges was only observed with dynamic baking (ramp rate of 50˚C/min) and a short 15 s spin coat duration. Dynamically baked films spun for 60 s showed a more planar and granular morphology. Similar to the previous work, the dynamically baked nano-ridged structure showed the best performance due primarily to an increased FF and shunt resistance (R_{SH}). The best P3HT:PC_{61}BM device showed a PCE of 3.59% and the device based on a BHJ containing the low band gap polymer poly(thienothiophene-co-benzodithiophene)7-F20 (PTB7-F20) blended with [6,6]-phenyl C71 butyric acid methyl ester (PC_{71}BM) achieved a PCE as high as 6.42%.[3]

It is apparent from the works referenced above that ETL morphology and properties are highly dependent on the specific combination of conditions used for the sol gel method. Significant changes in ZnO morphology can also affect the overlying active layer coating quality. This is often overlooked as the active layer conditions were held constant for different ETL morphologies and conditions in the previous studies. Thus, it is important to investigate the optical field distribution throughout the device as the ETL changes and to actively optimize the BHJ layer conditions in order to achieve the optimal device performance as the underlying ETL morphology changes.

Journal of Materials Chemistry A Accepted Manuscript

Large leaps in OPV efficiency have been realized in recent years through the development of low band gap semiconducting polymers, such as PTB7.[18] High efficiency inverted devices using a BHJ of PTB7:$PC_{71}BM$ have shown improvement with fine control and treatment of the bottom ETL and the top hole collecting layers reaching PCEs exceeding 8%.[6, 7] However, it is often seen in the literature that the control devices using sol gel ZnO and PTB7:$PC_{71}BM$ active layers only achieve PCEs in the 5-7% range.[13, 19] Experimental conditions may vary widely leading to a broad range in performance between very similar devices in the literature. Therefore, in high efficiency systems, it is especially important to ensure that control devices are fully optimized in order to illuminate the full benefits that newly engineered modifications (e.g. surface treatments, additives, nanostructuring, etc.) can provide.

In this work, the ZnO ETL morphology was controlled and studied for optimization in high efficiency inverted OPVs based on the PTB7:$PC_{71}BM$ BHJ. The sol gel precursor concentration, spin coating speed and baking conditions were used to simultaneously control the film thickness and morphology of ZnO films. The optical properties for each condition were measured and used in transfer matrix method (TMM) calculations to evaluate their effect on device performance. The calculated optical field distributions for completed devices are discussed in conjunction with the measured ZnO morphology and thicknesses and active layer conditions. The average PCE for planar and nano-ridged ZnO films of varied thickness was consistently high at 7.65-8.01% for all conditions, in contrast to other studies, with a maximum PCE reaching 8.32%. This insensitivity of device performance to ZnO variations is discussed in the context of the small domain microstructures of the PTB7:$PC_{71}BM$ active layer as well as the rapid intramolecular charge separation and highly efficient photovoltaic function of PTB7. In

Journal of Materials Chemistry A Accepted Manuscript

addition, the need for fine control of the active layer thickness as underlying ZnO layer morphology changes is highlighted as the primary variable for achieving high performance.

2. Results and Discussion

2.1 Morphology and Optical Properties of ZnO Films with Varied Processing Conditions

ZnO films were prepared using the sol gel method with different precursor concentrations, spin coating speeds and baking conditions. As seen in Table 1, ZnO film thickness was steadily increased as the precursor concentration was increased while fixing the spin coating speed or as the spin coating speed was decreased while fixing the precursor concentration. ZnO nano-ridges are clearly observed when using the dynamic baking condition. For each combination, the average film thickness of the nano-ridged and planar ZnO films is approximately the same while the roughness of the nano-ridged samples is expectedly higher. The average film thickness varies from 40-64 nm for all the conditions used here. For dynamically baked ZnO thin films, the spin coating speed and precursor concentration not only alter the film thickness but also the height and density of the nano-ridges themselves as shown in the AFM topography images in Fig. 1(a) and (b). For films from the 0.54 M precursor solution, the nano-ridges spin coated at 2000 rpm are significantly taller (e.g. peaks up to ~70 nm) than those spin coated at 4000 rpm (e.g. peaks up to ~38 nm). This is clearly shown in the cross-sectional topography graphs in Fig. 1(e) and (f) and reflected in the measured root mean square (RMS) roughness values of 12.80 nm vs. 8.83 nm (Table 1). The valley-to-valley distance between the nano-ridges averaged ~650 nm for the films spun at 2000 rpm and ~370 nm for those spun at 4000 rpm. The same trend was observed for dynamically baked films made from the 0.44 M precursor solution. Conversely, the statically baked films show similar planar morphologies (Fig. 1(c) and (d)) for all precursor concentrations and spin coating speeds but

Journal of Materials Chemistry A Accepted Manuscript

vary primarily in film thickness (Table 1). Film surface roughness varies with the precursor concentration even at the same spin speed. RMS roughness values varied with solution concentration by up to ~0.8 nm for the static films and ~1.1 nm for the dynamic films.

Table 1. The film number, ZnO precursor solution concentration, spin coating speed, and baking condition with the resulting film thickness as determined by spectroscopic ellipsometry and the root mean square (RMS) roughness (Rq) from AFM.

Film #	Precursor Concentration (M)	Spin Speed (rpm)	Bake Condition	Film Thickness (nm)	R_q (nm)
1S	0.44	4000	Static	42	4.16
1D	0.44	4000	Dynamic	40	7.76
2S	0.54	4000	Static	48	3.40
2D	0.54	4000	Dynamic	47	8.83
3S	0.44	2000	Static	52	3.00
3D	0.44	2000	Dynamic	55	13.30
4S	0.54	2000	Static	62	2.59
4D	0.54	2000	Dynamic	64	12.80

Journal of Materials Chemistry A Accepted Manuscript

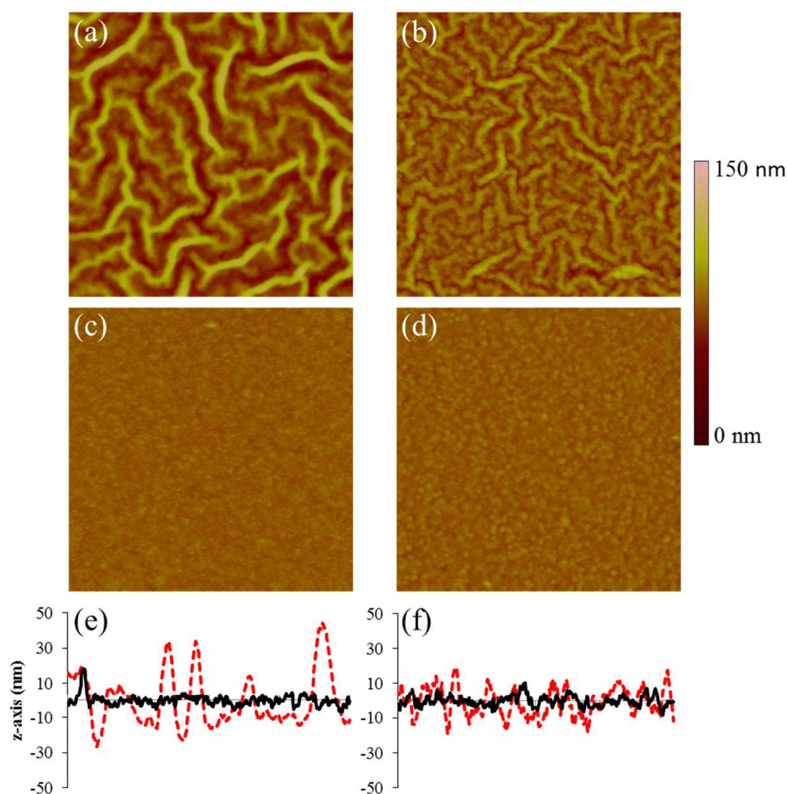

Figure 1. Tapping mode AFM topography images (5 µm x 5 µm) of ZnO sol gel films with processing conditions (a) 2000 rpm, dynamic bake; (b) 4000 rpm, dynamic bake; (c) 2000 rpm, static bake; (d) 4000 rpm, static bake. Height scale for all is 150 nm. All images are for films made with a precursor sol gel solution concentration of 0.54 M. (e) and (f) Line profile of a 4 µm trace measured across (a, c) and (b, d), respectively. The red dotted lines are the cross sections of (a) and (b), respectively. The solid black lines are the cross sections of (c) and (d), respectively.

Journal of Materials Chemistry A Accepted Manuscript

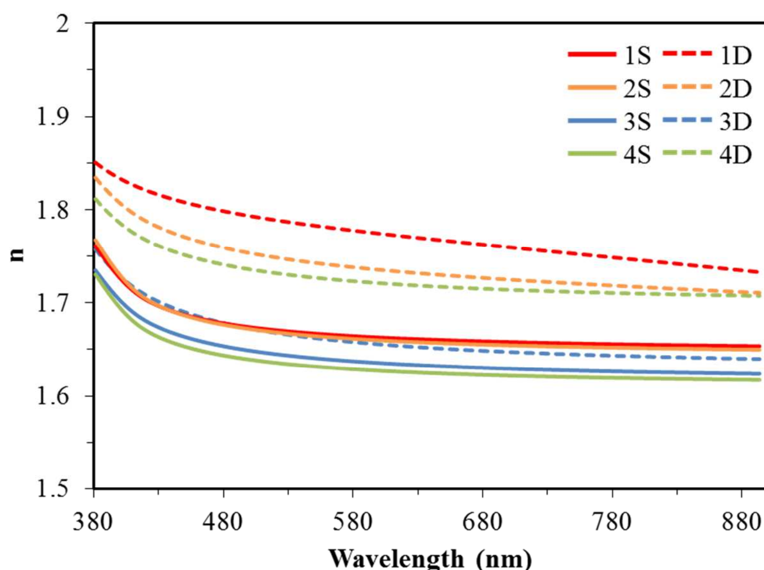

Figure 2. The refractive indices for various statically baked (solid lines) and dynamically baked (dotted lines) ZnO films with different thicknesses and morphologies. The film numbers in the legend correspond to the films listed in Table 1.

The optical properties of the ZnO thin films were investigated using UV-Vis-NIR absorption spectroscopy and spectroscopic ellipsometry. The films are highly transparent in the visible region above 400 nm and an onset of absorption is near the band gap of ZnO at ~370 nm (see Fig. S1 in the Supporting Information).[1] Additional light scattering is apparent for the nano-ridged film due to increased surface roughness. Figure 2 shows the refractive indices (n) of the ZnO films prepared under the different conditions listed in Table 1. The refractive index of these films varies from approximately 1.6-1.85 in the visible region. For statically baked films, those spun at 4000 rpm (i.e. films #1S and 2S) show a very similar refractive index of ~1.66 at 600 nm, as do those spun at 2000 rpm (i.e. films #3S and 4S) with ~1.63 at 600 nm. Although a higher precursor concentration can result in a thicker film under the same spin coating speed, the refractive indices of these films are similar. The slightly higher refractive indices of films produced at the higher spin coating speed could be due to the high packing density of the film

Journal of Materials Chemistry A Accepted Manuscript

caused by the higher compacting force during the spin process. For the dynamically baked films, a similar trend of spin coating speed on the refractive index was observed. The ZnO films with smaller nano-ridges produced by spin coating at 4000 rpm (i.e. films #1D and 2D) show higher refractive indices of 1.74-1.77 at 600 nm compared to those with larger nano-ridges produced by spin coating at 2000 rpm (i.e. films #3D and 4D) with 1.66-1.72 at 600 nm. Unlike the insensitivity to the precursor concentration for films prepared under the static baking conditions, the refractive indices of these nano-ridged films changes significantly with the precursor concentration at the same spin coating speed. The presence of residual solvent molecules in the precursor films and a slower solvent drying rate facilitate the formation of nano-ridges.[3] The slower drying rate caused by the dynamic baking process amplifies the effects of varied solution concentration on the film morphology and packing and thereby the refractive index. The crystallinity of thin films can also affect their refractive indices. The crystallization of ZnO in the films prepared by this sol gel method begins at 200-300˚C.[12] Formation of highly crystalline ZnO films requires baking at high temperatures of 450-800˚C.[11, 12, 17, 20] Yang et al. observed the X-ray diffraction (XRD) peaks corresponding to the (100), (002) and (101) crystal planes of ZnO with sol-gel derived films baked at 500˚C on SiO_2 substrates.[2] However, these peaks were not observed for the same films baked at 200˚C and the films were ascribed to having composite amorphous character. Park et al. also made sol-gel derived ZnO films baked at 200˚C on silicon (100) substrates and only faintly observed these crystalline peaks.[3] Since all the films produced in this work were baked at 200˚C for 1 hour, the crystallinity should be similar. Therefore, the refractive index variations could mainly be due to the difference in morphology and packing density of each film.

Journal of Materials Chemistry A Accepted Manuscript

With the sol gel method, the heat treatment conditions affect the vaporization of the solvents, the decomposition of zinc acetate and the crystallization of ZnO which in turn affect the structural relaxation of the gel film and the optical properties of the film. Therefore, the refractive index of ZnO films varies with both the baking conditions and the chosen solvents and precursors.[12] The index of refraction of a material is related to its density and may be lowered by non-scattering porosity.[21] Based on the measured refractive indices, calculation of the relative density of these films showed that, for both static and dynamic baking, the 4000 rpm condition provides denser films (see Table S1 in the Supporting Information).[12, 21] Additionally, the dynamically baked films show higher relative densities than the statically baked ones suggesting that the slower drying condition leads to structural relaxation and more densely packed ZnO films.

2.2 Characterization and Optical Modeling for Devices with Statically Baked ZnO ETL

The ZnO films prepared by varied conditions listed in Table 1 were deployed in inverted OPVs using the PTB7:$PC_{71}BM$ active layer. Figure 3 shows a schematic of the OPV device structure and the current-voltage curves for such devices with statically baked (i.e. planar) ZnO films made with 0.44 and 0.54 M concentrations at 2000 and 4000 rpm. The film thickness and RMS roughness of films prepared under these conditions are listed in Table 1. The surface roughness increases slightly as the film thickness decreases. The performance parameters of these devices are summarized in Table 2. The average active layer film thickness for these devices is ~94 nm. The devices with planar ZnO films all behaved very similarly even as the ZnO thickness increased from ~42 to ~62 nm. The J_{SC} for these devices was approximately the same with averages ranging from 14.17 to 14.50 mA/cm^2. The V_{OC}'s and FF's were also very consistent for these devices averaging 0.75 V and 72.3-73.4%, respectively, resulting in

Journal of Materials Chemistry A Accepted Manuscript

repeatably high PCE's averaging 7.65-8.01% with a maximum of 8.32% observed. The consistently high performance is shown in Fig. 3 as the curves of the best devices for each statically baked ZnO condition are essentially the same. This consistently high performance occurs in spite of the small drop in refractive index between the 1S and 2S versus the 3S and 4S ZnO films mentioned earlier. Thus, the thickness and small roughness variations in these planar ZnO films do not significantly affect the performance of these inverted OPV devices.

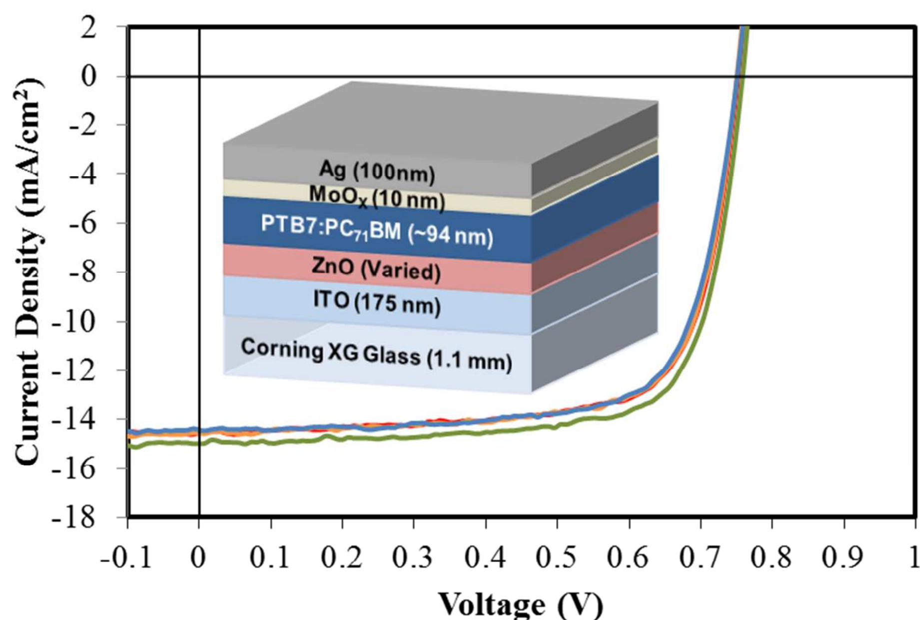

Figure 3. J-V curves for organic solar cells with statically baked ZnO layers corresponding to films # 1S (red), 2S (orange), 3S (blue), and 4S (green) in Table 1. The inset shows a schematic of the device.

Journal of Materials Chemistry A Accepted Manuscript

Journal of Materials Chemistry A Accepted Manuscript

Table 2. Average parameters of the inverted OPV devices with statically baked ZnO films indicated by the film numbers listed in Table 1.

ZnO Film	V_{OC} (V)	FF (%)	J_{SC} (mA/cm^2)	PCE (%)	PCE_{max} (%)
1S	0.75 +/- 0.00	72.7 +/- 0.5	14.44 +/- 0.25	7.83 +/- 0.15	7.99
2S	0.75 +/- 0.01	72.6 +/- 0.5	14.19 +/- 0.39	7.70 +/- 0.23	7.96
3S	0.75 +/- 0.00	72.3 +/- 0.4	14.17 +/- 0.44	7.65 +/- 0.26	7.92
4S	0.75 +/- 0.00	73.4 +/- 0.6	14.50 +/- 0.28	8.01 +/- 0.19	8.32

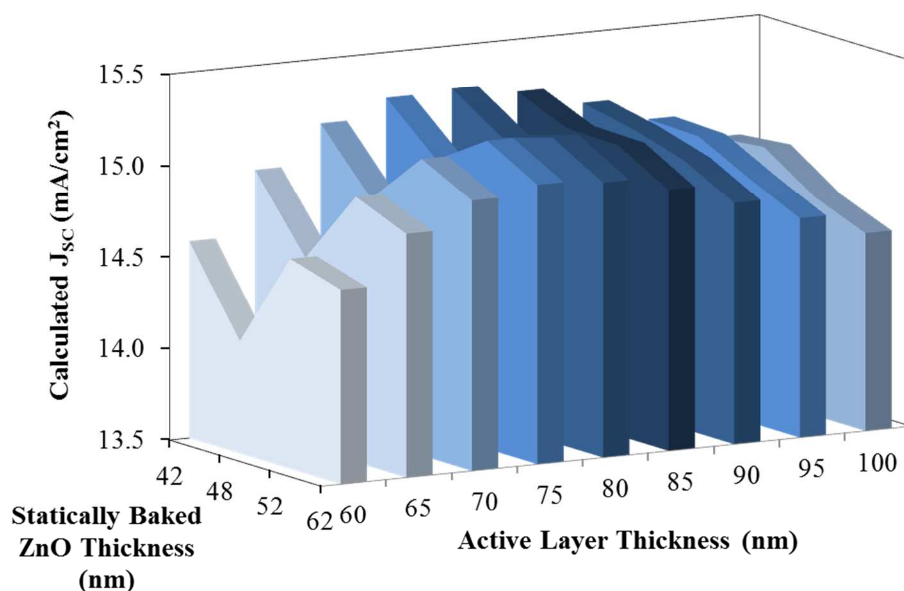

Figure 4. TMM calculations showing the change in J_{SC} versus thickness of statically baked ZnO and active layers.

TMM calculations were performed to explore the effect of different ZnO films prepared under statically baked conditions on the optical distribution and charge generation in devices. Figure 4 shows the TMM calculations of the device J_{SC} as a function of the ZnO film thickness for films made under static baking as well as a function of the active layer thickness. The refractive index of each ZnO film was experimentally measured, shown in Fig. 2, and used in the TMM simulations. The difference in ZnO films makes a relatively larger impact on J_{SC} for

devices with thinner active layers but is still within ~0.5 mA/cm^2. The thickness of the planar ZnO films in the devices is in the range of approximately 42 to 62 nm. Within this range, Figure 4 shows the calculated J_{SC} varies from 14.7 to 15.1 mA/cm^2 for a 94 nm active layer (i.e. the approximate PTB7:$PC_{71}BM$ thickness of devices in Fig. 3), which is close to the experimental J_{SC}. Figure 4 shows that both the ZnO and the active layer thicknesses require simultaneous optimization to achieve maximum photocurrent.

Device performance independent of film thickness for planar ZnO films was also observed in the study of inverted BHJ devices with the P3HT:$PC_{61}BM$ active layer.[14] As an ETL, the ZnO film should completely cover the ITO electrode to prevent current leakage. Once complete coverage is achieved, the thickness of the film has little effect on performance regardless of whether the active layer is P3HT:$PC_{61}BM$ or PTB7:$PC_{71}BM$. However, the surface roughness of ZnO films affects the device performance in different ways when the active layer is P3HT:$PC_{61}BM$ versus PTB7:$PC_{71}BM$. For P3HT:$PC_{61}BM$ BHJ devices, the increase of surface roughness from 2.86 to 4.02 nm resulted in the decrease of FF from 56 to 44%, accompanied by the increase of series resistance (R_S) from 10.7 to 31.7 Ω cm^2.[14] It was suggested that a rougher ZnO film surface could induce more small voids between the P3HT:$PC_{61}BM$ active layer and the ZnO layer. In contrast, a consistently high FF of 72.3-73.4% was displayed in our devices regardless of the roughness variation from 2.59 to 4.16 nm among the four statically baked ZnO films. This may be due to differences in the microstructure and other properties of the PTB7:$PC_{71}BM$ system compared to the P3HT:$PC_{61}BM$ system. For example, the P3HT:$PC_{61}BM$ system has optimal performance with a microstructure consisting of large and highly crystalline polymer domains that have distinct phase separation with PCBM. This type of BHJ relies on increased carrier mobility within the crystalline polymer domains and higher order

Journal of Materials Chemistry A Accepted Manuscript

for better connected charge transport pathways to counterbalance its less efficient photovoltaic function.[22] The PTB7:$PC_{71}BM$ BHJ, on the other hand, is a largely amorphous film with single polymer strands connecting multiple small separate crystalline domains and a relatively high PCBM content to ensure a continuous acceptor network for efficient charge collection.[22] This morphology combined with significant intramolecular charge separation due to PTB7's in-chain donor-acceptor copolymer structure creates rapid charge separation and highly efficient photovoltaic function.[22] Thus, these smaller domains and the higher intrinsic PV function of the PTB7-based system appear to desensitize these devices to small roughness variations in the underlying ZnO films.

2.3 Characterization of Devices with Dynamically Baked ZnO ETL

We also fabricated devices using the four dynamically baked ZnO films to observe the effect of the extreme morphology change from the planar films to those with the smaller and larger nano-ridges. Figure 5 shows the current-voltage curves of devices made on the four dynamically baked ZnO films. The 1D and 2D films are spun at 4000 rpm with thicknesses of ~40 nm and ~47 nm, respectively, while the 3D and 4D films are spun at 2000 rpm with thicknesses of ~55 nm and ~64 nm, respectively. The inset of Fig. 5 shows the AFM image of the device top surface area outside the electrode, i.e. on MoO_3 of the stack of glass/ITO/ZnO (3D)/PTB7:$PC_{71}BM$/MoO_3, for a device with the large ZnO nano-ridges. The underlying texture of the ZnO nano-ridges can be seen protruding through the subsequent layers. The protrusion of the ZnO nano-ridges through the active layer suggests that these structures may affect the coating of the active layer on top. Thus, for a given ZnO film condition, it is important to ensure that the active layer coating conditions are adjusted to maintain the optimum thickness. At the similar BHJ thickness of ~94 nm, the J-V curves for the 1D, 2D, 3D and 4D ZnO conditions are all very

Journal of Materials Chemistry A Accepted Manuscript

similar and these devices showed high performance with average PCEs ranging from 7.68-7.79% and a maximum PCE of 8.14% (see Table 3). Congruent to the devices with the planar ZnO films, these PTB7-based devices with ZnO nano-ridges are not sensitive to the overall effective ZnO thickness or roughness as long as the thickness of the active layer is maintained.

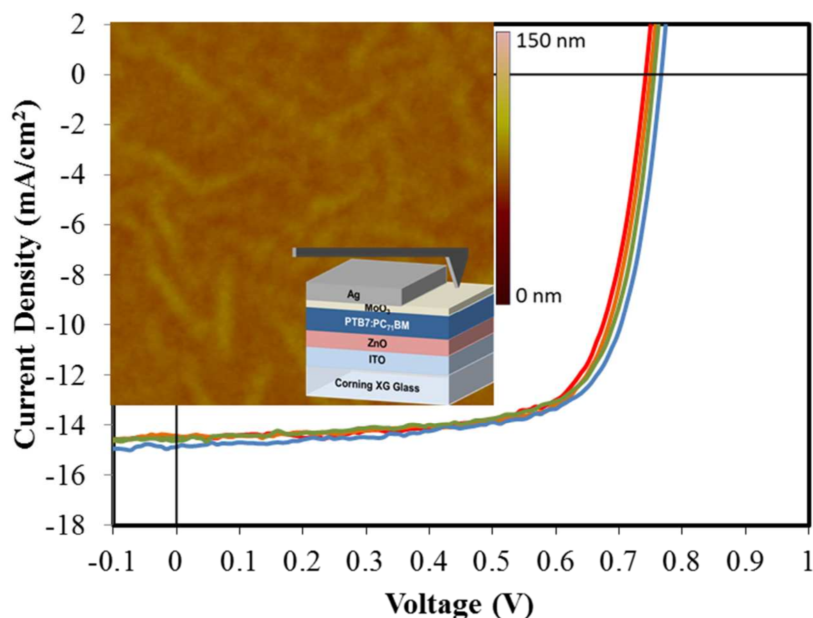

Figure 5. The J-V curves for devices with dynamically baked ZnO films of 1D (red), 2D (orange), 3D (blue) and 4D (green). The inset shows the AFM height image of a device on the MoO_3 layer outside the electrode area (i.e. ITO/ZnO (3D)/PTB7:PC_{71}BM /MoO_3). The AFM images are 5µm x 5µm.

Table 3. Parameters of the inverted OPV devices with dynamically baked ZnO films indicated by the film numbers in Table 1.

ZnO Film	V_{OC} (V)	FF (%)	J_{SC} (mA/cm^2)	PCE (%)	PCE_{Max} (%)
1D	0.74 +/- 0.00	72.9 +/- 0.3	14.22 +/- 0.29	7.68 +/- 0.14	7.83
2D	0.74 +/- 0.00	72.9 +/- 0.7	14.27 +/- 0.33	7.74 +/- 0.18	7.99
3D	0.75 +/- 0.01	72.4 +/- 0.7	14.32 +/- 0.43	7.79 +/- 0.28	8.14
4D	0.76 +/- 0.00	70.7 +/- 1.1	14.51 +/- 0.18	7.78 +/- 0.16	7.90

Journal of Materials Chemistry A Accepted Manuscript

We observed that there is no significant difference in the performance of the devices with the ZnO nano-ridges versus the planar films for similar PTB7:$PC_{71}BM$ layer thickness. Comparing devices with ZnO films 3S versus 3D (see Tables 2 and 3), for example, the FF's are practically equal at 72.3% and 72.4%, respectively, and the J_{SC}'s are very close at 14.17 and 14.32 mA/cm^2, respectively, allowing both to exhibit high average PCE's near 8%. Additionally, the EQE spectra for these devices show no significant difference between those using planar and nano-ridged ZnO layers (see Fig. S2 in the Supporting Information). However, for P3HT:$PC_{61}BM$ based devices, different device performance was observed using nano-ridged versus planar ZnO films.[10] The increased FF observed in those P3HT:$PC_{61}BM$ devices was attributed to higher electron selectivity and more efficient charge collection due to the nano-ridged structure. Larger nano-ridges were formed in those ZnO films (~120 nm in height) with the condition of a higher precursor concentration (0.75 M). Also, the electronic properties of those ZnO films may differ from ours due to higher crystallinity created by the increased baking temperature of 275˚C. Another study baked ZnO films at the lower temperature of 200˚C, which is the same as is used in this work, but also observed the nano-ridged devices performed better with the P3HT:$PC_{61}BM$ BHJ.[3] Similar to the discussion of planar devices in the previous section, our observations of the PTB7-based devices versus those for P3HT-based ones can be explained by the differences in microstructure and inherent PV function between these two systems. The rapid charge separation and highly efficient photovoltaic function of the PTB7:$PC_{71}BM$ BHJ provide high FF's consistently exceeding 70% when the active layer thickness is optimized. This effectively desensitizes this OPV system to the ZnO conditions probed here. Park et al. also compared planar and nano-ridged ZnO films in a PTB7-F20:$PC_{71}BM$ BHJ, similar to the devices presented in this work.[3] They observed slight increases

Journal of Materials Chemistry A Accepted Manuscript

in all performance parameters to reach a PCE of 6.42% with the nano-ridges versus 5.12% with the planar films. However, this relatively low PCE and FF of 65% for the nano-ridged device suggest the active layer thickness was not fully optimized. Additionally, differences between PTB7 and PTB7-F20 as well as between their ZnO film conditions versus ours may also contribute to these observations.

2.4 Optimization of Active Layer for Different ZnO ETL Morphologies

It is well known that active layer film thickness is crucial to optimizing performance in OPV devices. Organic semiconductors have relatively low charge carrier mobilities which limits the active layer thickness in most OPV devices to less than ~100 nm.[23-25] The optimum thickness reflects a balance between maximizing light absorption and minimizing charge recombination. Additionally, overall light harvesting in OPVs is closely related to the electric field distribution and intensity within the completed device architecture which is tied to the thickness and optical properties of each layer.

We performed TMM calculations to investigate how the optimum active layer thickness changes for the ZnO films prepared under different conditions. The experimentally measured refractive indices of each ZnO film (see Fig. 2) were used in the TMM calculations. Figure 6(a) shows the calculated J_{SC} versus active layer thickness for each of the ZnO films. According to the TMM results, the active layer film thickness dominates the behavior of the J_{SC}. Varying the ZnO film thickness and morphology do not significantly change the optimum active layer film thickness for these inverted devices. The J_{SC} maxima of 15.0-15.3 mA/cm^2 for the various ZnO films are predicted with the active layer thickness primarily centered between ~75-95 nm. As we have observed for devices made on different ZnO films (Tables 2 and 3), similar J_{SC}'s (14.17-14.51 mA/cm^2) and FF's (70.7-73.4%) were obtained as long as the active layers had similar

Journal of Materials Chemistry A Accepted Manuscript

thickness (~94 nm). The model assumes 100% internal quantum efficiency (IQE) and does not take recombination or parasitic resistances into account. Thus, the model predicts in general that thicker active layers would generate higher J_{SC}'s.

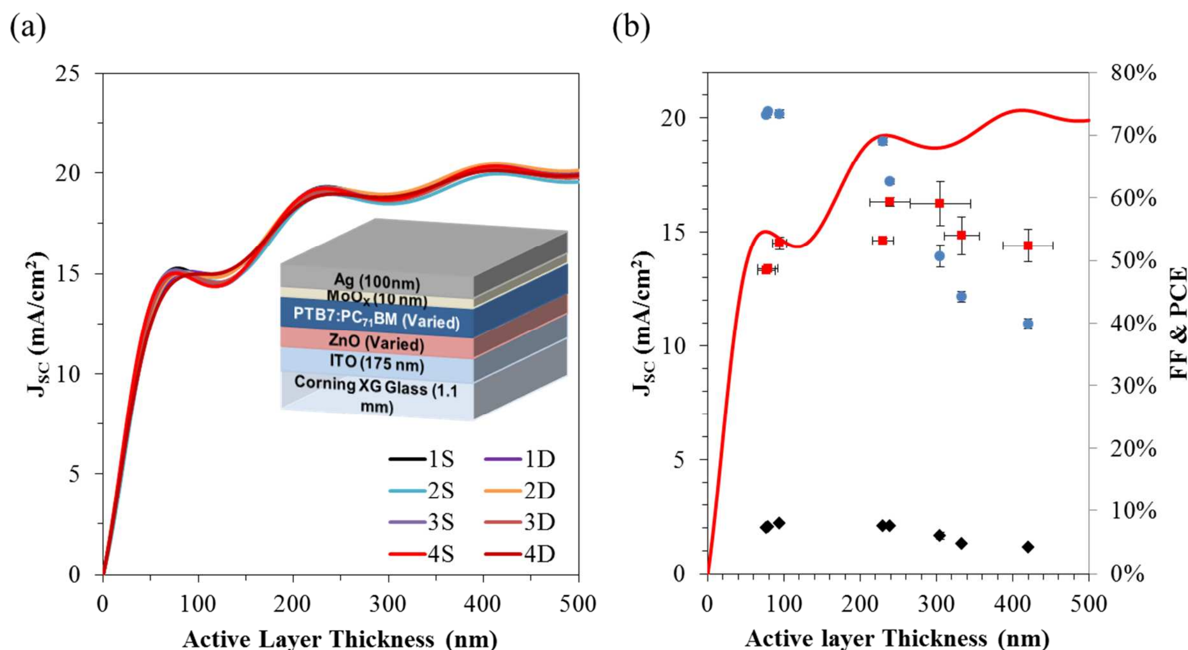

Figure 6. (a) The calculated J_{SC} versus active layer thickness for each of the ZnO films, as labeled in Table 1, using their respective optical properties. The inset shows a schematic of the device structure modeled. (b) The calculated (red line) versus experimental (red squares) J_{SC} for devices of varied active layer thickness with a statically baked ZnO film (4S). The experimental FF (blue circles) and PCE (black triangles) of the devices are also included.

Devices with varied active layer thicknesses were fabricated on top of statically baked ZnO films for comparison. The ZnO films were prepared with the same condition for 4S in Table 1. Figure 6(b) shows the experimental J_{SC}'s (red squares) of these devices compared to the calculated J_{SC}'s (red line). The J-V curves and the performance parameters for these devices are provided in Fig. S3 and Table S2 in the Supporting Information. The average J_{SC} for the actual devices was 14.50 mA/cm^2 (Table 2) versus the calculated J_{SC} of 14.70 mA/cm^2 at an optimal active layer thickness of ~94 nm. The experimental value is expected to be slightly lower than

Journal of Materials Chemistry A Accepted Manuscript

the calculated value as real devices do not operate at 100% IQE and suffer losses due to recombination and parasitic resistances. Variation may also be introduced due to any error in the measured experimental film thicknesses and refractive indices. When the active layer was increased to ~240 nm, the experimental J_{SC} did increase to 16.31 mA/cm^2 but at the cost of a diminished FF which dropped from 73.4% to 62.6%. This drop in FF is due to the thicker active layer requiring charges to travel further to reach their respective electrodes which increases the recombination probability. Even though the thicker active layer generated an increased J_{SC}, the large FF decrease resulted in a drop of the average PCE from 8.01% to 7.54%. The lower experimental J_{SC} compared to the calculated Jsc for the thicker active layer is also a direct result of high recombination rates. Further increasing the active layer thickness to ~305 nm, ~333 nm, and ~420 nm resulted in declining FF's of 50.7%, 44.2%, and 39.9% resulting in PCEs of 5.98%, 4.74%, and 4.15%, respectively. The J_{SC}'s also dropped to 16.24 mA/cm^2, 14.84 mA/cm^2, and 14.40 mA/cm^2, respectively. Figure 6 shows that the TMM calculations predict a sharp variation of J_{SC} in either direction near the optimum active layer thickness (i.e. ~75-95 nm). Moving the opposite direction and decreasing the active layer to ~79 nm maintained a high FF at 73.7% but showed the J_{SC} drop to 13.40 mA/cm^2 resulting in an average PCE of 7.39%. This highlights the sensitivity of these devices to small changes in active layer thickness. Large changes in ZnO morphology may affect the thickness of the active layer spun on top. Thus, it is important to ensure that the active layer coating conditions are adjusted to maintain the optimum thickness when changing the underlying ZnO conditions.

3. Conclusions

In conclusion, we fabricated high efficiency inverted devices using the PTB7:$PC_{71}BM$ BHJ and studied the effects of varied ZnO ETL morphology and thickness on device

Journal of Materials Chemistry A Accepted Manuscript

performance. By statically and dynamically baking the ZnO, we created planar and nano-ridged structures, respectively. The optical properties of the various ZnO films were measured and also observed to change with morphology. Optical calculations showed that optical field distribution changes due to the different ZnO films could only account for small changes in J_{SC} in the range of 0.3-0.5 mA/cm^2. In agreement with the models, devices fabricated with statically baked, planar ZnO films of varied conditions showed consistent J_{SC}'s ranging from 14.17-14.50 mA/cm^2. These devices were insensitive to the varied ZnO thickness and roughness and exhibited consistently high PCEs averaging 7.65-8.01% with a maximum PCE reaching 8.32%. The devices fabricated here also showed no significant difference in performance between those with planar versus nano-ridged ZnO ETLs which also exhibited high PCE's averaging 7.68-7.79% with a maximum PCE reaching 8.14%. The highly efficient photovoltaic function of the PTB7:$PC_{71}BM$ BHJ provides consistently high FF's exceeding 70%, when the active layer thickness is optimized, effectively desensitizing this OPV system to the ZnO conditions probed here. However, the models and experiments highlight the sensitivity of these devices to active layer film thickness. Thus, maintaining the optimum active layer thickness when changing the underlying ETL conditions is critical for achieving high efficiency inverted OPVs.

4. Experimental

4.1 Film and Device Fabrication

The ZnO sol-gel solution was prepared by dissolving zinc acetate dihydrate ($Zn(CH_3COO)_2 \cdot 2H_2O$, Sigma-Aldrich, >99.0%, 1 g for 0.44 M, 0.5 g for 0.54 M) and ethanolamine ($NH_2CH_2CH_2OH$, Sigma-Aldrich, >99.5%, 0.277 mL for 0.44 M, 0.1375 mL for 0.54 M) in 2-methoxyethanol ($CH_3OCH_2CH_2OH$, Sigma-Aldrich, 99.8%, anhydrous, 10 mL for 0.4 4M, 4.1 mL for 0.54 M) under vigorous stirring for greater than 12 h. ITO-coated glass

Journal of Materials Chemistry A Accepted Manuscript

substrates were used for all films and devices and were first cleaned by ultrasonication in soapy deionized (DI) water, DI water, acetone, and isopropanol. The substrates were treated with oxygen plasma prior to depositing any films. The ZnO solutions were then spin-cast on top of the pre-cleaned ITO-glass substrates at either 2000 or 4000 rpm for 60 s. These samples were then annealed at 200℃ for 1 hour under dynamic or static conditions. For static baking, the substrates were placed directly on a hot plate at 200℃ and baked for 1 hour. For dynamic baking, the substrates sat at room temperature for 10-15 minutes and were then placed on a hot plate at room temperature which was ramped to 200℃ over 1 minute, after which the substrates were baked for 1 hour. A PTB7 solution (1-Material, Inc.; 20.7 mg/mL) and a $PC_{71}BM$ solution (Nano-C; 31.0 mg/mL) in chlorobenzene were each made in a N_2-filled glovebox and stirred overnight at 60℃. Then these solutions were mixed with a polymer:fullerene ratio of 1.5:1 with 3.0 vol% 1,8-diiodooctane and allowed to stir for >1 hour. The mixed solution was then cooled to room temperature and filtered with a 0.2 μm PTFE filter. The cooled filtered solution was spincast on top of the ZnO films at varied rpms for 60 s. Then, the active layer coated substrates were loaded in a vacuum chamber ($<10^{-6}$ Torr) where a 10 nm film of MoO_3 and 100 nm film of Ag was deposited through a shadow mask by thermal evaporation. Each substrate had 4 pixels with defined areas of 10 mm^2 each.

4.2 Film and Device Characterization

Morphology images of the ZnO films and on top of the MoO_3 layer but outside the electrode area of the finished devices were taken by AFM in tapping mode (Bruker/Veeco/DI Multimode AFM-2). The thickness of the active layers on bare ITO glass was measured by profilometry (KLA Tencor Alpha-Step 500). UV-Vis-NIR absorption spectra of ZnO films were obtained using a Perkin Elmer Lambda 900 UV-Vis-NIR absorption spectrometer.

Journal of Materials Chemistry A Accepted Manuscript

The refractive index, extinction coefficients, and thicknesses of the various ZnO films and of the other layers in the devices were measured with spectroscopic ellipsometry (J.A. Woollam Co., Inc. α-SE Spectroscopic Ellipsometer, CompleteEASE software). All ZnO films of the various conditions were made on glass/ITO substrates for characterization with ellipsometry, AFM, and absorption spectroscopy. Ellipsometry measurements were first made on bare glass (Corning XG) and then on bare glass/ITO substrates in order to build the optical models for these substrates. The Cauchy dispersion relation was used to model the optical parameters of the bare glass substrates. An index-graded layer was used to model the optical properties of the ITO layers, which is typical, along with the known ITO thickness from the substrate manufacturer. The parameters for the glass and ITO layers were held constant as the parameters were calculated for the overlying ZnO layers. Black tape was applied to the backside of the glass for all samples to eliminate errors from backside reflections. The depolarization was ensured to be near zero for all measurements indicating that little light is reflected from the backside into the detector. The ZnO optical parameters were found using a B-Spline fit which works well for materials that are partially transparent and partially absorbing. The fit parameters were ensured to be physical by ensuring that k was greater than or equal to zero, assuming a transparent region and band gap of 3.3 eV (i.e. the band gap of ZnO), and maintaining Kramers-Kronig consistency between the e1 and e2 spline curves. An effective roughness layer was added to the models to account for non-idealities due to surface roughness features. The root mean squared error values were ensured to be less than 20 which is reasonable for samples with much structure and oscillation in the measured data.

Current-voltage measurements for all inverted devices were conducted in a glove box under nitrogen atmosphere using a Keithley 2400 Source Meter and a solar simulator with a

Journal of Materials Chemistry A Accepted Manuscript

Solar Light Co. Xenon lamp (16S-300W) and an AM 1.5 filter. The light intensity was calibrated to 100 mW/cm^2 using a calibrated silicon solar cell that had been previously standardized at the National Renewable Energy Laboratory. EQE measurements were gathered in air using an Oriel Xenon lamp (450W) with an AM1.5 filter, a monochromator (Oriel Cornerstone 130 1/8 m), and a lock-in amplifier (Stanford Research Systems).

4.3 Optical Modeling

The transfer matrix method (TMM) was used to calculate the optical field distribution within devices and to estimate the potential photocurrent produced in the active layer.[26] TMM calculates the interference of reflected and transmitted light waves at each interface in the stack based on each materials optical properties as represented by their complex refractive index ($\tilde{n} = n + ik$). The refractive indices (n) and extinction coefficients (k) of the various layers used in the models were measured with spectroscopic ellipsometry. The TMM calculations were run based on the device architectures discussed using the film thickness, n, and k that were measured for each ZnO film. The TMM calculations assume planar layer interfaces and isotropy for all the films. The interference is assumed incoherent within the glass substrates because their thicknesses (1.1 mm) are much higher than the wavelengths of the simulated incident light.

Acknowledgements

This work was supported by the National Science Foundation (NSF) (CBET-1346859). Device fabrication and performance measurements were carried out in the UW Department of Chemistry's Photonics Research Center. AFM measurements were conducted in Professor Shaoyi Jiang’s research lab. UV–vis–NIR absorption measurements were carried out in the UW

Journal of Materials Chemistry A Accepted Manuscript

Department of Chemistry's Spectroscopic and Analytical Instrumentation Facility. EQE measurements were conducted in the lab of Professor Alex Jen.

Appendix A. Supporting Information

Supplementary data associated with this article can be found online.

References

1. Y. M. Sun, J. H. Seo, C. J. Takacs, J. Seifter and A. J. Heeger, *Adv. Mater.*, 2011, **23**, 1679-+.
2. T. B. Yang, W. Z. Cai, D. H. Qin, E. G. Wang, L. F. Lan, X. Gong, J. B. Peng and Y. Cao, *Journal of Physical Chemistry C*, 2010, **114**, 6849-6853.
3. H. Y. Park, D. Lim, K. D. Kim and S. Y. Jang, *Journal of Materials Chemistry A*, 2013, **1**, 6327-6334.
4. Z. A. Tan, W. Q. Zhang, Z. G. Zhang, D. P. Qian, Y. Huang, J. H. Hou and Y. F. Li, *Adv. Mater.*, 2012, **24**, 1476-1481.
5. S. K. Hau, H. L. Yip, N. S. Baek, J. Y. Zou, K. O'Malley and A. K. Y. Jen, *Appl Phys Lett*, 2008, **92**.
6. Z. C. He, C. M. Zhong, S. J. Su, M. Xu, H. B. Wu and Y. Cao, *Nat. Photonics*, 2012, **6**, 591-595.
7. S. M. Yoon, S. J. Lou, S. Loser, J. Smith, L. X. Chen, A. Facchetti and T. J. Marks, *Nano Letters*, 2012, **12**, 6315-6321.
8. S. K. Hau, H. L. Yip, H. Ma and A. K. Y. Jen, *Appl Phys Lett*, 2008, **93**, 233304.
9. S. K. Hau, H. L. Yip, O. Acton, N. S. Baek, H. Ma and A. K. Y. Jen, *J. Mater. Chem.*, 2008, **18**, 5113-5119.
10. N. Sekine, C. H. Chou, W. L. Kwan and Y. Yang, *Org. Electron.*, 2009, **10**, 1473-1477.
11. S. Y. Kuo, W. C. Chen and C. P. Cheng, *Superlattices and Microstructures*, 2006, **39**, 162-170.
12. M. Ohyama, H. Kozuka and T. Yoko, *Thin Solid Films*, 1997, **306**, 78-85.
13. L. Krishnan Jagadamma, M. Abdelsamie, A. El Labban, E. Aresu, G. O. Ngongang Ndjawa, D. H. Anjum, D. Cha, P. Beaujuge and A. Amassian, *Journal of Materials Chemistry A*, 2014.
14. Z. Q. Liang, Q. F. Zhang, O. Wiranwetchayan, J. T. Xi, Z. Yang, K. Park, C. D. Li and G. Z. Cao, *Advanced Functional Materials*, 2012, **22**, 2194-2201.
15. Y. J. Lin and C. L. Tsai, *J Appl Phys*, 2006, **100**, 4.
16. B. J. Richardson, L. Z. Zhu and Q. M. Yu, *Sol Energ Mat Sol C*, 2013, **116**, 252-261.
17. R. Castanedo-Perez, O. Jimenez-Sandoval, S. Jimenez-Sandoval, J. Marquez-Marin, A. Mendoza-Galvan, G. Torres-Delgado and A. Maldonado-Alvarez, *Journal of Vacuum Science & Technology a-Vacuum Surfaces and Films*, 1999, **17**, 1811-1816.
18. Y. Y. Liang, Z. Xu, J. B. Xia, S. T. Tsai, Y. Wu, G. Li, C. Ray and L. P. Yu, *Adv. Mater.*, 2010, **22**, E135-+.
19. M. Thambidurai, J. Y. Kim, J. Song, Y. Ko, H. J. Song, C. M. Kang, N. Muthukumarasamy, D. Velauthapillai and C. Lee, *Journal of Materials Chemistry C*, 2013, **1**, 8161-8166.
20. J. M. Khoshman and M. E. Kordesch, *Thin Solid Films*, 2007, **515**, 7393-7399.
21. B. E. Yoldas and D. P. Partlow, *Thin Solid Films*, 1985, **129**, 1-14.
22. J. M. Szarko, B. S. Rolczynski, S. J. Lou, T. Xu, J. Strzalka, T. J. Marks, L. P. Yu and L. X. Chen, *Advanced Functional Materials*, 2014, **24**, 10-26.
23. K. S. Chen, H. L. Yip, J. F. Salinas, Y. X. Xu, C. C. Chueh and A. K. Y. Jen, *Adv. Mater.*, 2014, **26**, 3349-+.

Journal of Materials Chemistry A Accepted Manuscript

24. G. Li, R. Zhu and Y. Yang, *Nat. Photonics*, 2012, **6**, 153-161.
25. J. Nelson, *Materials Today*, 2011, **14**, 462-470.
26. G. F. Burkhard, E. T. Hoke and M. D. McGehee, *Adv. Mater.*, 2010, **22**, 3293-+.

Graphical Abstract

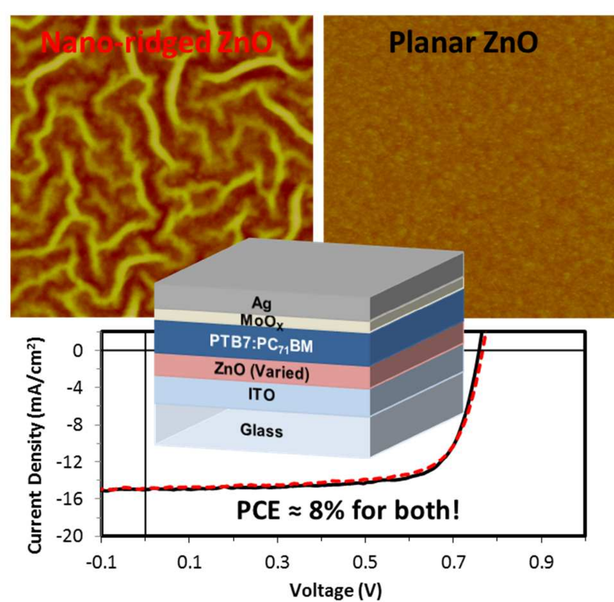

Journal of Materials Chemistry A Accepted Manuscript